Ocean Sci., 3, 17–30, 2007
www.ocean-sci.net/3/17/2007/

Ocean Science

Overturning cells in the Southern Ocean and subtropical gyres

J. A. Polton and D. P. Marshall

Department of Meteorology, University of Reading, UK

Received: 19 June 2006 – Published in Ocean Sci. Discuss.: 21 July 2006
Revised: 25 October 2006 – Accepted: 17 November 2006 – Published: 26 January 2007

Abstract. The circulation of the subtropical gyres can be decomposed into a horizontal recirculation along contours of constant Bernoulli potential and an overturning circulation across these contours. While the geometry and topology of Bernoulli contours is more complicated in the subtropical gyres than in the Southern Ocean, these subtropical overturning circulations are very much analogous to the overturning cell found in the Southern Ocean. This analogy is formalised through an exact integral constraint, including the rectified effects of transient eddies. The constraint can be interpreted either in terms of vertical fluxes of potential vorticity, or equivalently as an integral buoyancy budget for an imaginary fluid parcel recirculating around a closed Bernoulli contour. Under conditions of vanishing buoyancy and mechanical forcing, the constraint reduces to a generalised non-acceleration condition, under which the Eulerian-mean and eddy-induced overturning circulations exactly compensate. The terms in the integral constraint are diagnosed in an eddy-permitting ocean model in both the North Pacific subtropical gyre and the Southern Ocean. The extent to which the Eulerian-mean and eddy-induced overturning circulations compensate is discussed in each case.

1 Introduction

The circulation in the Southern Ocean can be decomposed, at a conceptual level, into the quasi-zonal recirculation of the Antarctic Circumpolar Current (ACC), and overturning circulation across the ACC. In steady state this averaging technique results in the adiabatic and fictitious overturning called the Deacon cell. It is a balance where the Eulerian-mean flow is exactly cancelled by transient and standing eddy-induced overturnings. No density changes are involved and the apparent deep cell is the result of superimposing multiple recirculations on zonally inclined isopycnals (Döös and Webb, 1994). While being an idealisation, this decomposition allows one to consider the three-dimensional circulation as the superposition of two quasi two-dimensional cells.

In the ACC, the streamwise averaged Eulerian-mean overturning circulation is dominated by the wind-driven northward flow in the surface Ekman layer, and compensating geostrophic southward flow at depth. However, the Lagrangian-mean overturning circulation, taking into account the rectified effects of transient geostrophic eddies, can look rather different. In the absence of buoyancy forcing the streamwise Eulerian-mean and eddy-induced overturning circulations cancel, corresponding to non-acceleration conditions (Eliassen and Palm, 1961; Plumb, 1990). More generally, the equilibrium residual circulation is controlled by buoyancy forcing (Marshall, 1997; Speer et al., 2000; Karsten et al., 2002; Gallego et al., 2004), with quasi-adiabatic upwelling of North Atlantic Deep Water and subduction of Antarctic Intermediate and Bottom waters. This residual overturning circulation has been termed the "diabatic Deacon cell" by Speer et al. (2000) and includes the what is traditionally called the thermohaline circulation.

In the Southern Ocean standing eddies contribute to the streamwise averaged Eulerian-mean flow, hereafter Eulerian mean flow, and are responsible for the observed Deacon cell (Stevens and Ivchenko, 1997). By exerting a drag on the mean flow standing eddies vertically transmit zonal momentum from the surface to the bottom topography. In subtropical gyres a Deacon cell does not appear, in the zonal average, since pressure gradients at lateral boundaries can balance the applied wind forcing. However we argue that isopycnic circulations can appear as an adiabatic Deacon cell when averaging around closed Bernoulli contours.

Hence an equivalent decomposition can be effected for the closed gyres found in the subtropical (and subpolar) basins. While the topology of the geostrophic streamlines is more

Correspondence to: J. A. Polton
(jpolton@ucsd.edu)

Published by Copernicus GmbH on behalf of the European Geosciences Union.

complex than in the Southern Ocean, using precisely the same principles, the flow can be rigorously decomposed into a recirculating gyre flow along closed Bernoulli contours, and an overturning circulation across the Bernoulli contours.

In both the Southern Ocean and the subtropical gyres, it is worth cautioning that the overturning cells and the recirculating geostrophic flow cannot be considered truly independent of each other. In order to see this, even when the thermohaline circulation are excluded, consider the spin-up of the ACC in response to an eastward wind stress at the sea surface. The wind stress generates an equatorward Ekman transport which, in order to maintain continuity, is quickly balanced by a poleward geostrophic flow at depths beneath the Drake Passage and upwelling over the Southern Ocean. This upwelling and compensating downwelling to the north of the ACC steepens the isopycnals, leading to a zonal transport through thermal-wind balance. This process is ultimately arrested either when slumping of the isopycnals by baroclinic instability and/or surface buoyancy forcing (or friction) is able to compensate for the steepening of the isopycnals by the Deacon cell (Johnson and Bryden, 1989; Karsten et al., 2002; Speer et al., 2000). Thus there is strong coupling between the strength of the overturning cell and the recirculating geostrophic flow. Inclusion of thermohaline effects from overturning in the ocean basins further complicates the dynamics, see Rintoul et al. (2001). This is graphically illustrated with iconic figure of Schmitz (1996, Fig. II-8 p22) where the Southern Ocean is depicted as the hub of the world's ocean basins coupling overturning circulations with the ACC.

The overturning circulation in the subtropical gyres must necessarily have a diapycnal component and so must differ from that in the Southern Ocean. However, the wind-induced coupling of the overturning and recirculating flow can be expected to behave in an analogous manner, as described in the following. The surface wind stress generates convergent Ekman flow at the surface and hence Ekman downwelling. This downwelling will pump the isopycnals downwards (Luyten et al., 1983), leading to geostrophic recirculation at depth through thermal-wind balance. This process can only be arrested once diapycnal mixing and/or baroclinic eddies are able to compensate for this downward pumping of the isopycnals (Marshall et al., 2002). Thus a key issue is whether the Eulerian-mean and eddy-induced components of the subtropical overturning cells largely compensate, leading to non-acceleration conditions.

These physical arguments can be formalised through an integral constraint applied along a closed Bernoulli contour at a fixed depth (Marshall, 2000) which has some similarities with the classical residual mean framework. However, this new constraint can also accommodate the deep NADW-AABW cell of the Southern Ocean where the water mass transformation occurs in subpolar gyres that cannot be adequately described using the residual mean theory. The integral constraint we present can either be interpreted as a buoyancy budget following a fluid parcel recirculating around the Bernoulli contour, or equivalently as an integral budget on the vertical flux of potential vorticity within that contour. Such budgets have been investigated in a planetary-geostrophic ocean model of a subtropical gyre by Polton and Marshall (2003). In this paper we extend the theory to include the effects of transient eddies and we illustrate the relation between the meridional overturning cells in the Southern Ocean and the overturning cells across the mean Bernoulli streamlines in the subtropical gyres by evaluating these budgets within an eddy-permitting ocean model.

The paper is structured as follows. In Sect. 2, the theoretical background is reviewed and extended to incorporate the rectified effects of transient eddy fluxes of potential vorticity, and we also discuss the relation of these potential vorticity fluxes to the overturning circulation across the mean geostrophic streamlines. In Sect. 3 we briefly summarise the numerical ocean model and the methods used to evaluate the terms in the integral budgets. In Sect. 4 these diagnostics are evaluated over the ACC and interpreted in terms of the classical overturning cell. In Sect. 5, these diagnostics are then evaluated over the subtropical gyre of the North Pacific, and interpreted in terms of the overturning circulation across the closed geostrophic streamlines. Finally in Sect. 6 we present a brief concluding discussion.

2 Theoretical background

2.1 Potential vorticity flux

Decomposing the variables into time-mean ($\overline{X}$) and time-varying components (X') using a suitable time-filtering operator, the time-mean momentum equation for a rotating, hydrostatic, Boussinesq fluid can be written in vector form as

$$\frac{\partial \overline{\boldsymbol{v}}}{\partial t} + \overline{\boldsymbol{q}} \times \overline{\boldsymbol{u}} + \nabla \tilde{\Pi} = \overline{\boldsymbol{F}} + \boldsymbol{F}_R - \frac{\overline{\Delta\rho}}{\rho_0} g \boldsymbol{k}, \tag{1}$$

where

$$\boldsymbol{F}_R = -\overline{\boldsymbol{q}' \times \boldsymbol{u}'} - \nabla \frac{\overline{\boldsymbol{v}' \cdot \boldsymbol{v}'}}{2}$$

is the force associated with the Reynolds stresses, i.e., the rectified effects of transient eddies in Eq. (1), and

$$\tilde{\Pi} = \frac{\overline{p}}{\rho_0} + \frac{\overline{\boldsymbol{v}} \cdot \overline{\boldsymbol{v}}}{2} + gz$$

is the Bernoulli potential calculated using the mean pressure and mean velocity.[1] Here $\boldsymbol{u}=(u, v, w)$ and $\boldsymbol{v}=(u, v, 0)$,

$$\boldsymbol{q} = 2\boldsymbol{\Omega} + \nabla \times \boldsymbol{v}$$

is the absolute vorticity, $\boldsymbol{\Omega}$ is the rotation vector, $\nabla=(\partial/\partial x, \partial/\partial y, \partial/\partial z)$, g is the gravitational acceleration,

[1] Alternatively, $\overline{\boldsymbol{v}' \cdot \boldsymbol{v}'}/2$ can be included in $\tilde{\Pi}$ rather than $\boldsymbol{F}_R$.

$\rho=\rho_0+\Delta\rho$ is the density where ρ_0 is a reference density, $\boldsymbol{k}$ is a vertical unit vector, p is the pressure, z is height, and $\boldsymbol{F}$ represents all horizontal mechanical body forces.

Similarly, a time-mean buoyancy equation can be written

$$\frac{\partial\overline{\sigma}}{\partial t}+\overline{\boldsymbol{u}}\cdot\nabla\overline{\sigma}=\overline{\mathcal{B}}-\nabla\cdot\overline{\boldsymbol{u}'\sigma'}, \quad (2)$$

where σ is potential density (relative to a suitable reference level; more generally one could interpret σ as a neutral density; McDougall, 1987), $\overline{\mathcal{B}}$ represents buoyancy forcing, and $\overline{\boldsymbol{u}'\sigma'}$ is the eddy potential density flux.

Following White and Bromley (1995) a potential vorticity law can be obtained for a hydrostatic, Boussinesq fluid. An analogous law can be stated as a function of time-mean variables:

$$\rho_0\frac{\overline{D}\tilde{Q}}{Dt}=-\overline{q}\cdot\nabla(\overline{\mathcal{B}}-\nabla\cdot\overline{\boldsymbol{u}'\sigma'})-\nabla\overline{\sigma}\cdot\nabla\times(\overline{\boldsymbol{F}}+\boldsymbol{F}_R-\frac{\overline{\Delta\rho}}{\rho_0}g\boldsymbol{k}), \quad (3)$$

where $\frac{\overline{D}}{Dt}=\frac{\partial}{\partial t}+\overline{\boldsymbol{u}}\cdot\nabla$, and

$$\tilde{Q}=-\frac{\overline{\boldsymbol{q}}\cdot\nabla\overline{\boldsymbol{\sigma}}}{\rho_0} \quad (4)$$

is a modified potential vorticity flux defined in terms of time averaged vorticity and potential density. Note the minus sign in Eq. (4) is such that the large scale potential vorticity is positive in the Northern Hemisphere.

This can be reexpressed in flux form

$$\frac{\partial}{\partial t}(\rho_0\tilde{Q})+\nabla\cdot\tilde{J}=0, \quad (5)$$

where

$$\tilde{J}=\rho_0\tilde{Q}\overline{\boldsymbol{u}}+\overline{\boldsymbol{q}}(\overline{\mathcal{B}}-\nabla\cdot\overline{\boldsymbol{u}'\sigma'})+(\overline{\boldsymbol{F}}+\boldsymbol{F}_R-\frac{\overline{\Delta\rho}}{\rho_0}g\boldsymbol{k})\times\nabla\overline{\sigma}+\nabla\times\boldsymbol{A} \quad (6)$$

is defined up to an arbitrary $\nabla\times\boldsymbol{A}$.

Taking the cross product of Eq. (1) with $\nabla\overline{\sigma}$ and eliminating $\overline{\boldsymbol{u}}\cdot\nabla\overline{\sigma}$ using Eq. (2), we obtain an alternative expression for $\tilde{J}$:

$$\tilde{J}=\nabla\tilde{\Pi}\times\nabla\overline{\sigma}+\overline{\boldsymbol{q}}\frac{\partial\overline{\sigma}}{\partial t}+\frac{\partial\overline{\boldsymbol{v}}}{\partial t}\times\nabla\overline{\sigma}-\nabla\times\boldsymbol{A}. \quad (7)$$

The new potential vorticity flux vector, $\tilde{J}$, constructed from time-mean variables, is distinct from the more familiar time mean of the *instantaneous* potential vorticity flux vector (Truesdell, 1951; Obukhov, 1962; Haynes and McIntyre, 1987, 1990). $\tilde{J}$ is constructed to preserve the steady state impermeability characteristic through $\tilde{\Pi}$ and $\overline{\sigma}$ surfaces, thus $\nabla\times\boldsymbol{A}=0$.

Making the Boussinesq assumption appears to have introduced a new gravity term that does not consistently sit in the definition for $\tilde{J}$. Its presence as a body force rather than a potential force is necessary for the conservation law to hold, but in the adiabatic scenario the flux vector does not simply reduce to an advective flux. However, using the Boussinesq approximation replaces a physical baroclinic solenoidal term, $\nabla\rho\times\nabla\sigma\cdot\nabla p$, (McDougall, 1987) that would otherwise appear in Eq. (3) with a nonvertical flux vector. This is convenient since we will only be interested in the vertical component of $\tilde{J}$.

2.2 Application of vertical potential vorticity flux

Following Marshall (2000), we can invoke the impermeability condition to eliminate the geostrophic type term, $\nabla\tilde{\Pi}\times\nabla\overline{\sigma}$, when we integrate over areas enclosed by Bernoulli contours at constant depth. Equating Eq. (6) and Eq. (7) and choosing $\nabla\times A=0$ we integrate the *vertical* components of the potential vorticity flux through the area enclosed by contours of constant Bernoulli potential at constant depth. Thus:

$$\iint_{\tilde{\Pi}}\left\{\tilde{J}_{\text{adv}}+\tilde{J}_{\text{buoy}}+\tilde{J}_{\text{fric}}+\tilde{J}_{\text{eddy}}+\tilde{J}_{\text{drift}}\right\}dA=0, \quad (8)$$

where

$$\tilde{J}_{\text{adv}} = \overline{\rho}\tilde{Q}\overline{w}, \quad (9)$$

$$\tilde{J}_{\text{buoy}} = \overline{q}^{(z)}\overline{\mathcal{B}}, \quad (10)$$

$$\tilde{J}_{\text{fric}} = \boldsymbol{k}\times\overline{\boldsymbol{F}}\cdot\nabla\overline{\sigma}, \quad (11)$$

$$\tilde{J}_{\text{eddy}} = \boldsymbol{k}\times\boldsymbol{F}_R\cdot\nabla\overline{\sigma}-\overline{q}^{(z)}\nabla\cdot(\overline{\boldsymbol{u}'\sigma'}), \quad (12)$$

$$\tilde{J}_{\text{drift}} = -\boldsymbol{k}\times\frac{\partial\overline{\boldsymbol{v}}}{\partial t}\cdot\nabla\overline{\sigma}-\overline{q}^{(z)}\frac{\partial\overline{\sigma}}{\partial t}. \quad (13)$$

Thus, in a statistically-steady state, the vertical component of the advective flux of potential vorticity must be compensated by either a buoyancy-forced, or a frictional potential vorticity flux (that includes the effects of wind forcing), or by an eddy-induced potential vorticity flux.

2.3 Approximate interpretation as a Lagrangian buoyancy budget

We now show how the potential vorticity flux constraint (8) can be related to a Lagrangian buoyancy budget following a fluid parcel circulating around a closed Bernoulli potential contour. In reality, the fluid parcel will not return to precisely its original position, but it will be displaced both vertically and laterally due to the overturning circulation across the closed Bernoulli contour, as sketched schematically in Fig. 1. In order to maintain a statistically-steady buoyancy field, this displacement must be balanced by buoyancy forcing and/or an eddy contribution to the buoyancy budget. To make this connection explicit, we consider the potential vorticity flux through an area bounded by two adjacent Bernoulli potential contours, $\tilde{\Pi}$ and $\tilde{\Pi}+\Delta\tilde{\Pi}$, as sketched in Fig. 2. We adopt natural coordinates whereby **s** and **n** are the unit vectors parallel and normal to the Bernoulli contours, and we assume that the dominant contribution to the fluid velocity comes from the horizontal recirculating component along Bernoulli contours, the magnitude of which we define as $\overline{v}_{\text{recirc}}$.

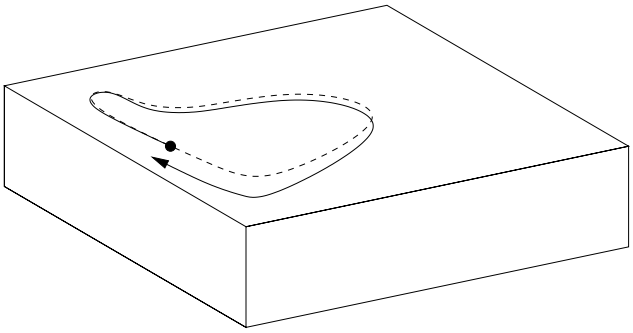

Fig. 1. A statistically steady Lagrangian trajectory does not exactly close due to diabatic processes. In a circuit it is displaced both vertically and laterally from its initial position.

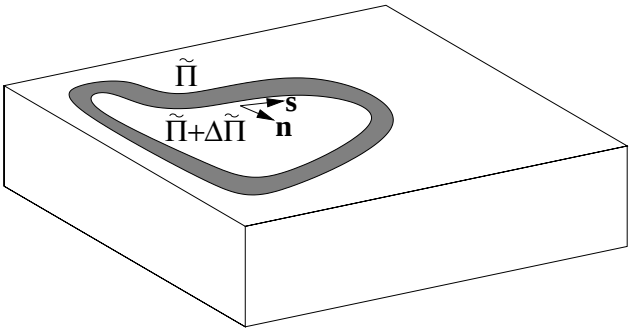

Fig. 2. Potental vorticity fluxes are integrated through a horizontal area bound by two adjacent closed Bernoulli potential contours, $\tilde{\Pi}$ and $\tilde{\Pi}+\Delta\tilde{\Pi}$.

To leading order, the horizontal component of the momentum Eq. (1) gives:

$$\overline{v}_{\text{recirc}} \approx \frac{1}{\overline{q}^{(z)}} \frac{d\tilde{\Pi}}{dn}.$$

We also have the kinematic relation

$$\overline{v}_{\text{recirc}} = \frac{ds}{dt}.$$

Thus the area element for the integration in natural coordinates can be written as

$$dA = ds\, dn \approx \frac{\Delta\tilde{\Pi}}{\overline{q}^{(z)}}\, dt.$$

Now, substituting for dA in Eq. (8) we can rewrite the integral constraint as an integral buoyancy budget around a closed Bernoulli contour:

$$\oint_{\tilde{\Pi}} \left\{ \frac{\partial\overline{\sigma}}{\partial t} + (\overline{\boldsymbol{v}} - \overline{\boldsymbol{v}}_{\text{recirc}} + \boldsymbol{v}^*).\nabla\overline{\sigma} + (\overline{w} + w^*)\frac{\partial\overline{\sigma}}{\partial z} - \overline{\mathcal{B}} \right\} dt \approx 0, \quad (14)$$

where $\boldsymbol{v}$ represents the horizontal velocity components and w the vertical velocity components. In deriving Eq. (14), we have assumed:

(i) the eddy-induced potential vorticity flux (12) can be represented as the advection of mean buoyancy by an eddy-induced velocity, $\mathbf{u}^*$ (Gent et al., 1995), where this velocity includes the contribution from the Reynolds stresses (Marshall et al., 1999);

(ii) the potential vorticity can approximated as

$$\tilde{Q} \approx -\frac{1}{\rho_0}\overline{q}^{(z)}\frac{\partial\overline{\sigma}}{\partial z}.$$

Thus, the integral constraint on the vertical flux of potential vorticity can be reinterpreted as a buoyancy budget following a fluid parcel recirculating around a closed Bernoulli potential contour. Since the recirculating component of the fluid velocity makes no contribution to this budget, the constraint therefore informs us about the mean residual overturning circulation, including the contribution from eddies.

2.4 Limiting regimes

What are the dominant balances in the integrated potential vorticity flux budgets that one can expect in the limits of purely wind-driven (adiabatic) and buoyancy-driven (diabatic) flows? Note that the sign of the potential vorticity flux is dependent on the hemisphere under consideration. Both of the limiting regimes discussed below are assumed to lie in the northern hemisphere; the signs of the potential vorticity fluxes should be reversed in the southern hemisphere.

2.4.1 Purely wind-driven flow

First consider an adiabatic flow subjected only to surface wind forcing, as sketched schematically in Fig. 3a. The wind stress and associated Ekman transport leads to an overturning cell across the mean Bernoulli contours that acts to steepen the isopycnals. As is evident from the figure, the upwelling arm of this overturning cell fluxes stratification, and hence potential vorticity, upwards, whereas the downwelling arm of the overturning cell fluxes stratification and potential vorticity downwards.

In a statistically-steady state, the steepening of the isopycnals is arrested by baroclinic instability, with an eddy-induced overturning cell acting to slump the isopycnals. Thus the eddy potential vorticity fluxes are in the opposite sense to the advective potential vorticity fluxes.

This is consistent with the integral constraint (Eq. 14) which, in the adiabatic limit of vanishing buoyancy forcing and a statistically-steady state, tells us that the net residual circulation across isopycnals must vanish. This limit corresponds to non-acceleration conditions (Eliassen and Palm, 1961; Plumb, 1990), and indeed the integral constraint (Eq. 8) might be interpreted as a non-acceleration theorem for non-zonal flows.

2.4.2 Purely buoyancy-driven flow

Conversely, consider the limit of a diabatic flow subjected only to surface buoyancy forcing, as sketched schematically in Fig. 3b. Cooling in the mixed layer destroys the surface stratification and is therefore equivalent to an upward potential vorticity flux.

In a statistically-steady state, and neglecting all mechanical forcing (including friction), the growth of the mixed layer is again arrested by baroclinic instability, with an eddy-induced overturning cell acting to slump the isopycnals as sketched in the figure. Within the mixed layer, where the eddies act to increase the temperature/buoyancy, the eddy potential vorticity flux is directed downward and opposes the buoyancy-forced potential vorticity flux.

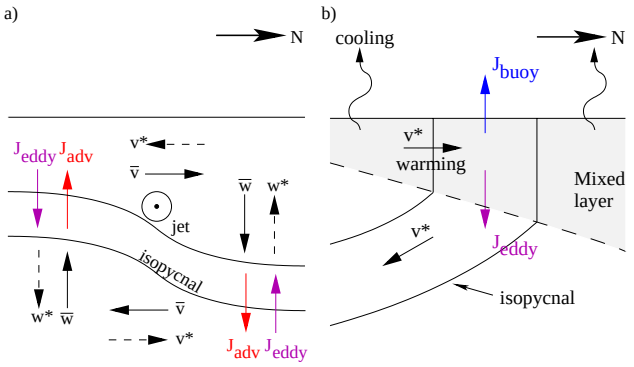

Fig. 3. Two limiting regimes corresponding to **(a)** purely wind-driven flow and **(b)** purely buoyancy-driven flow. Note that the potential vorticity flux vectors would have the opposite signs in the southern hemisphere.

3 Ocean model – overview and methodology

In the following sections, we present diagnostics from the OCCAM eddy-permitting ocean model (Webb et al., 1998). In Sect. 4 these diagnostics are evaluated over the Southern Ocean and in Sect. 5 they are evaluated over the North Pacific subtropical gyre. First, we briefly summarise the salient features of the ocean model and the methodology used to evaluate the integral potential vorticity flux budget terms.

3.1 Model data

OCCAM is an eddy-permitting global ocean general circulation model, integrated at $1/4°$ lateral resolution for 14 model years, with a 7 year spin-up phase followed by a 7 year analysis phase. The diagnostics are calculated from 3 year running means, during the analysis phase, of u, v, σ, $(u\sigma)$, $(v\sigma)$, potential temperature, salinity and sea surface height, and from 5 day averages at the start and finish of the 3 year averaging period of u, v and σ in order to calculate the mean tendencies. The term σ is a dimensionless potential density referenced to 2000 m.

In order to evaluate the Bernoulli potential, the in-situ density $\overline{\rho}$ is first calculated from the mean potential temperature and salinity fields using the equation of state. The pressure is then obtained from the density and sea surface height using hydrostatic balance.

3.2 Evaluation of potential vorticity fluxes

Consistent with the analysis in Sect. 2.3, the potential vorticity is also approximated to include only the mean vertical component of relative vorticity, such that

$$\tilde{Q} = -\frac{1}{\rho_0}\overline{q}^{(z)}\frac{\partial \overline{\sigma}}{\partial z}. \tag{15}$$

This approximation will lead to errors in the accuracy of the integral closure. The hydrostatic approximation has allowed us to discard vertical velocity ordinarily present in the Bernoulli potential.

The body force, $\overline{\boldsymbol{F}}$, is calculated as the residual of the momentum Eq. (1) since model data is not available for these terms. It includes the contribution from the Reynolds stresses and approximation errors in the simplification of $\tilde{Q}$. However, beneath the surface Ekman layer, the frictional potential vorticity flux, $\tilde{J}_{\text{fric}}$, makes a small contribution to the integral flux budget and is therefore not shown in the diagnostics.

The divergence of the eddy σ flux in $\tilde{J}_{\text{eddy}}$ (12), is approximated as the horizontal divergence,

$$\nabla \cdot \overline{\boldsymbol{u}'\sigma'} \approx \nabla \cdot \overline{\boldsymbol{v}'\sigma'}, \tag{16}$$

mainly since the vertical eddy potential density fluxes were not available. However, we note that the contribution from the vertical convergence of the vertical eddy potential density flux has been found to be small in previous studies (Roberts and Marshall, 2000), and this result can be expected on theoretical grounds if the eddies are quasi-geostrophic (Treguier et al., 1997). Any errors in this approximation are then absorbed into the mean buoyancy forcing, $\overline{\mathcal{B}}$, evaluated as a residual of the diagnosed terms in the time-mean potential density equation.

The steady state assumption is validated by calculating $\tilde{J}_{\text{drift}}$ at each depth and finding it to be very small. This means that the model is sufficiently spun up for the variables to be considered statistically-steady for the purpose of the diagnostics. Again these data are not shown.

3.3 Integration of potential vorticity fluxes

All of the variables are interpolated onto a $1/16°$ resolution grid for the purpose of evaluating the terms in the integral potential vorticity flux constraint (8) through an area bounded by adjacent Bernoulli contours. To facilitate comparison between potential vorticity fluxes between different Bernoulli contours, the results are presented as normalised

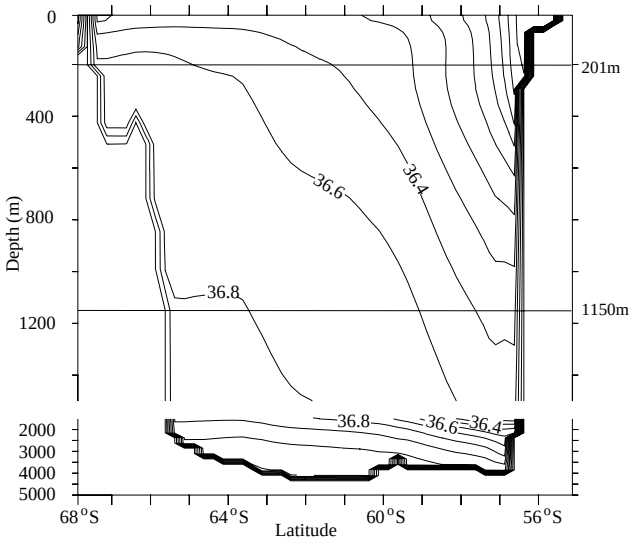

Fig. 4. A cross section of 3 year mean σ across the Drake passage at 69° W. A discussion is given for the analysis at depths of 201 m and 1150 m.

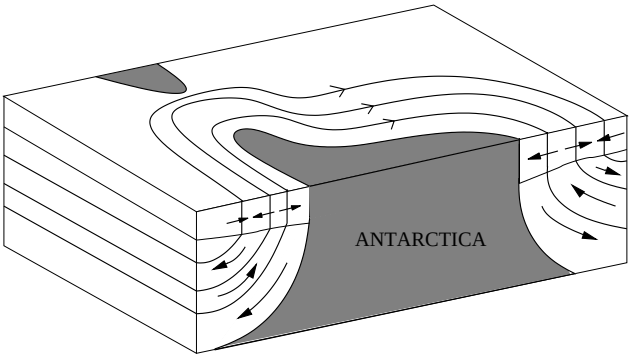

Fig. 5. Schematic of the residual overturning circulation across Bernoulli contours in the Southern Ocean. Water mass properties are set in the surface mixed later; beneath the mixed layer, water masses slide adiabatically over each other.

fluxes defined, for a general component, ζ, as

$$\tilde{J}_{\zeta}^{\tilde{\Pi}} = \lim_{\Delta\tilde{\Pi}\to 0} \frac{\int\int_{\tilde{\Pi}} \tilde{J}_{\zeta}\, dA}{\int\int_{\tilde{\Pi}} dA}. \tag{17}$$

In practice the largest and smallest Bernoulli contours that are closed around Antarctica (or the subtropical gyre) are found and the interval is evenly spaced in $\tilde{\Pi}$ into 20 closed contours. The sum of the terms in the integral constraint is found to be small and is therefore not shown in the presented diagnostics. In the following sections Figs. 7–8 and Figs. 11–13 are shaded and contoured in normalised potential vorticity flux values. The contours do not denote the 20 Bernoulli intervals as this was found to occlude the colour scheme in area of intensified flow. Instead the contour interval is chosen to aid the eye in separating the colours, and are plotted for every second colour interval, whilst showing the path of the Bernoulli contours.

4 Southern Ocean

The dynamics of the Southern Ocean meridional overturning cell has been widely documented elsewhere (Döös and Webb, 1994; Marshall, 1997; Speer et al., 2000; Rintoul et al., 2001; Karsten and Marshall, 2002; Olbers et al., 2004; Drijfhout, 2005). In this section, we present diagnostics of the potential vorticity fluxes at just two depths, 201 m and 1150 m, in order to demonstrate that integrating the fluxes leads to a great conceptual simplification and to demonstrate how these fluxes can be used to quantify the cancellation between the Eulerian-mean and eddy-induced overturning cells that results in subtropical overturning cells. For reference the two depths are shown in Fig. 4, superimposed on a section of σ across the Drake Passage.

The terms in the potential vorticity flux constraint tells us about the components of the overturning circulation directed across isopycnals, as evident from Eq. (14). In a statistically-steady state and in the absence of buoyancy forcing, one would expect the residual overturning circulation, including both the effects of the mean and eddy-driven flows, to vanish, consistent with the discussion in Sect. 2.4.1. However, surface buoyancy forcing leads to transformation of water masses within the surface mixed layer and their subduction/entrainment into/out of the ocean interior (Marshall, 1997; Speer et al., 2000). Beneath the mixed layer, these water masses can be expected to slide adiabatically along isopycnals, as sketched schematically in Fig. 5. At the two analysis depths, we can find evidence of each of the two idealised regimes sketched schematically in Fig. 3. Note that the potential vorticity fluxes presented in this section are in the opposite direction to their northern hemisphere counterparts, presented in the subtropical gyre discussion (Sect. 5) and in the limiting regimes discussion (Sect. 2.4).

4.1 201 m depth

To illustrate the capacity of the integral constraint to simplify the vertical potential vorticity fluxes we first present their components (9–12) and summation before horizontally integrating over closed contours. Figure 6 reveals a rich structure in all the steady fields (only the sign of the drift term 13 can be resolved using the same log scale, so is not shown). In particular the friction and total fluxes are locally non zero. However, when the integral is taken the utility of the integral constraint becomes apparent as the friction contribution self cancels and the total flux, by mathematical construction, also cancels. Figure 6 also shows qualitative values for the

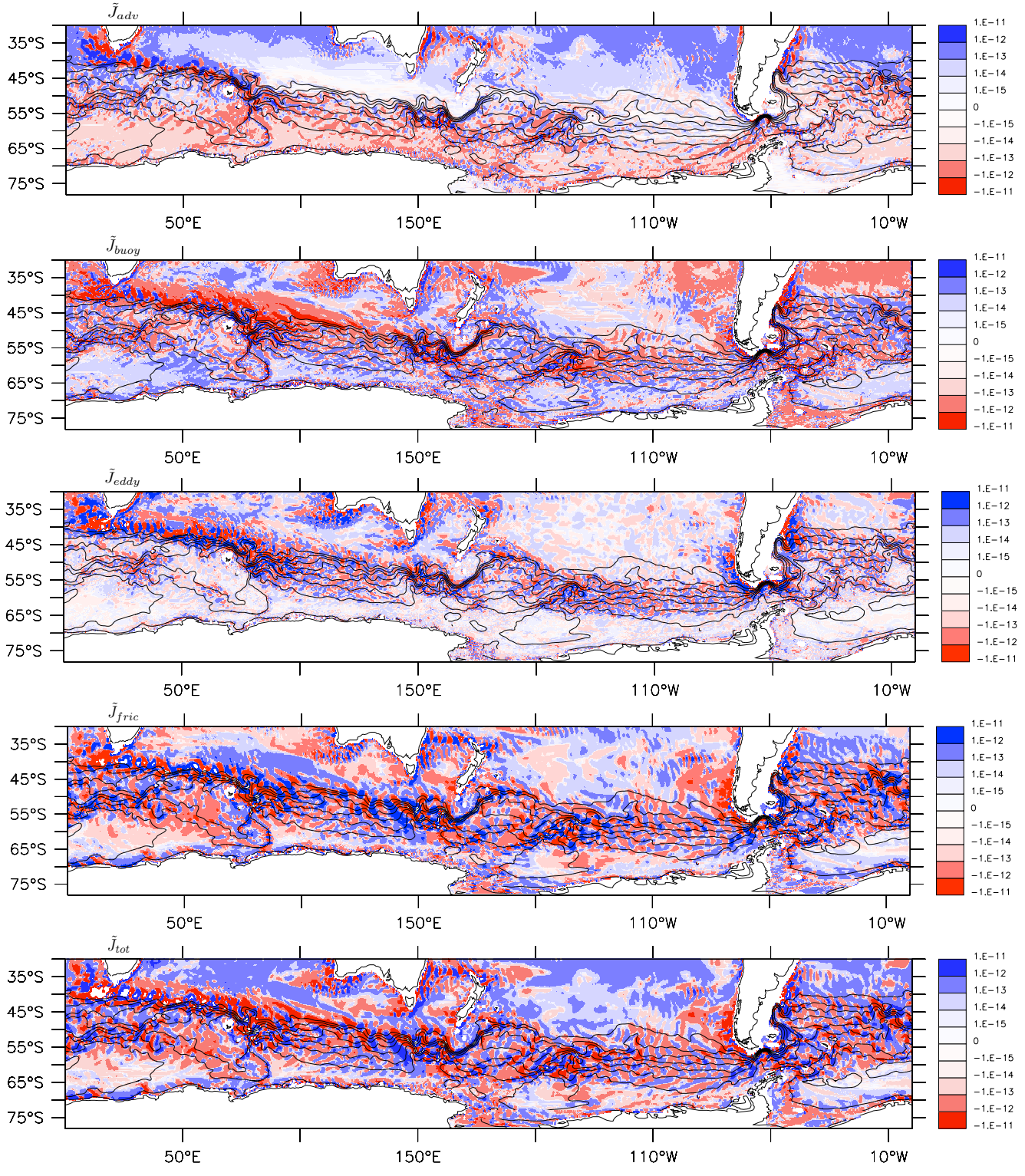

Fig. 6. Vertical components of potential vorticity flux (kg m^{-3} s^{-2}) at 201 m depth in the Southern Ocean. Contours are Bernoulli potential. The drift term is unresolvable on this scale so is not shown. Though there is complex spatial structure in all the components, integrating around closed Bernoulli contours necessarily results in a zero total flux and also reduces the balance to a three way expression between advection, buoyancy and eddy processes.

mean flow in the spacing of Bernoulli contours. In particular shaded quantities are occluded by stacked contours in regions of intensified flow. Consequently in the following analyses we present Bernoulli contours that are spaced in the normalised potential vorticity flux.

The upper analysis depth of 201 m lies within the lower part of the winter mixed layer and is therefore under the direct influence of surface buoyancy forcing, though beneath the surface Ekman layer and the direct influence of the wind forcing. We find a three-way balance between the vertical potential vorticity fluxes due to advection, buoyancy forcing and eddies. Figure 7 shows the fluxes integrated over the the area between the adjacent Bernoulli contours and normalized according to Eq. (17). The frictional, transient and total potential vorticity flux contributions to the integral balance are all sufficiently small such that only their signs would be resolved in the figure's colour log-scale, and are therefore not shown.

Over the northern part of the ACC, we find a positive advective potential vorticity flux associated with the downwelling limb of the Eulerian-mean overturning cell (note the sign change from the Northern Hemisphere case). This is opposed by a negative buoyancy-forced potential vorticity flux associated with surface cooling. Eddies also play a significant role, providing a net upward potential vorticity flux. Thus, far from cancelling the effect of the Eulerian-mean downwelling as sketched schematically in Fig. 3a, the eddies actually enhance the warm to cold water mass transformation at this depth. On the other hand, the eddies offset the effect of the surface cooling on the surface mixed layer, consistent with the limit sketched schematically in Fig. 3b.

Over the southern part of the ACC, the advective and eddy potential vorticity fluxes weakly oppose each other. The advective potential vorticity flux is negative, consistent with the upwelling of the Eulerian-mean overturning cell, whereas the eddy potential vorticity flux is positive, consistent with baroclinic slumping of the isopycnals (as sketched schematically in Fig. 3a) in the southern hemisphere. However, the cancellation between the Eulerian-mean and eddy-induced circulations is not complete, as there is a positive potential vorticity flux associated with buoyancy forcing. This is consistent with the net cold to warm water mass transformation of upwelled NADW into AAIW. Note that we see no evidence of a southward transformation of NADW into AABW over the southernmost part of the ACC. This is probably due to the known lack of significant AABW formation in the OCCAM model (Drijfhout, 2005).

This pattern of the buoyancy forcing, with warming over the southern part of the ACC and cooling over the northern part of the ACC is consistent with the discussion of Speer et al. (2000). They point out that eddies shed from the atmospheric polar jet will either transport warm air poleward or cold air equatorward; both scenarios will create a warming tendency poleward and a cooling equatorward of the jet, for an ocean and atmosphere that, in the absence of continental barriers, are in roughly in thermal equilibrium.

It is also worth commenting on the complementary analysis by Drijfhout (2005) using the same OCCAM model. He observes a large, uniformly poleward, eddy-induced transport over the surface layers of the ACC, dominated by the seasonal cycle of the mixed layer which acts to redistribute the Ekman transport over the seasonal thermocline. However, this process only arises when the eddy-induced transport is evaluated as the difference between the thickness-weighted mean isopycnal velocity and the Eulerian-mean velocity, and hence does not appear in the present analysis. When Drijfhout evaluates the eddy-induced velocities at fixed depths using residual-mean theory, he finds a uniform warm-to-cold eddy-induced transformation that only partially compensates for the Eulerian-mean overturning cell.

4.2 1150 m depth

At this deeper level (Fig. 8), there is near compensation between the negative advective potential vorticity flux and the positive eddy potential vorticity flux. The buoyancy-forced potential vorticity flux makes a small (and spurious) contribution, arising from the lateral diffusion of temperature and salinity employed in this version of OCCAM.

One might be tempted to argue that this compensation is consistent with a cancellation between the Eulerian-mean and eddy-induced overturning cells, as sketched schematically in Fig. 3a. However, this compensation can only be inferred for the components of the Eulerian-mean and eddy-induced cells directed across the mean isopycnals. Thus the present results are consistent with those obtained by Drijfhout (2005) who found only partial compensation between the Eulerian-mean and eddy-induced overturning cells, with a substantial residual directed along the isopycnals.

5 Subtropical gyre

We now turn to the subtropical overturning cells which we argue behave in an analogous manner to the overturning in the Southern Ocean. In order to illustrate the key concepts, we diagnose the various components of the vertical potential vorticity flux between adjacent Bernoulli potential contours in the subtropical gyre of the North Pacific. There is, however, an important distinction between the subtropical gyre flow and the ACC flow, which arises from mass conservation and the across-flow slope orientation of the isopycnals. Beneath the mixed layer, only the subtropical gyre requires a time-mean diapycnal mass flux in response to the Ekman pumping (compare Fig. 5 and Fig. 9). This process could be purely adiabatic if the eddy-induced circulation were to cancelled the Eulerian-mean contribution though in practice, as in the ACC, it is likely to be partially diffusive (diabatic) and partially eddy driven (adiabatic or diabatic). This has

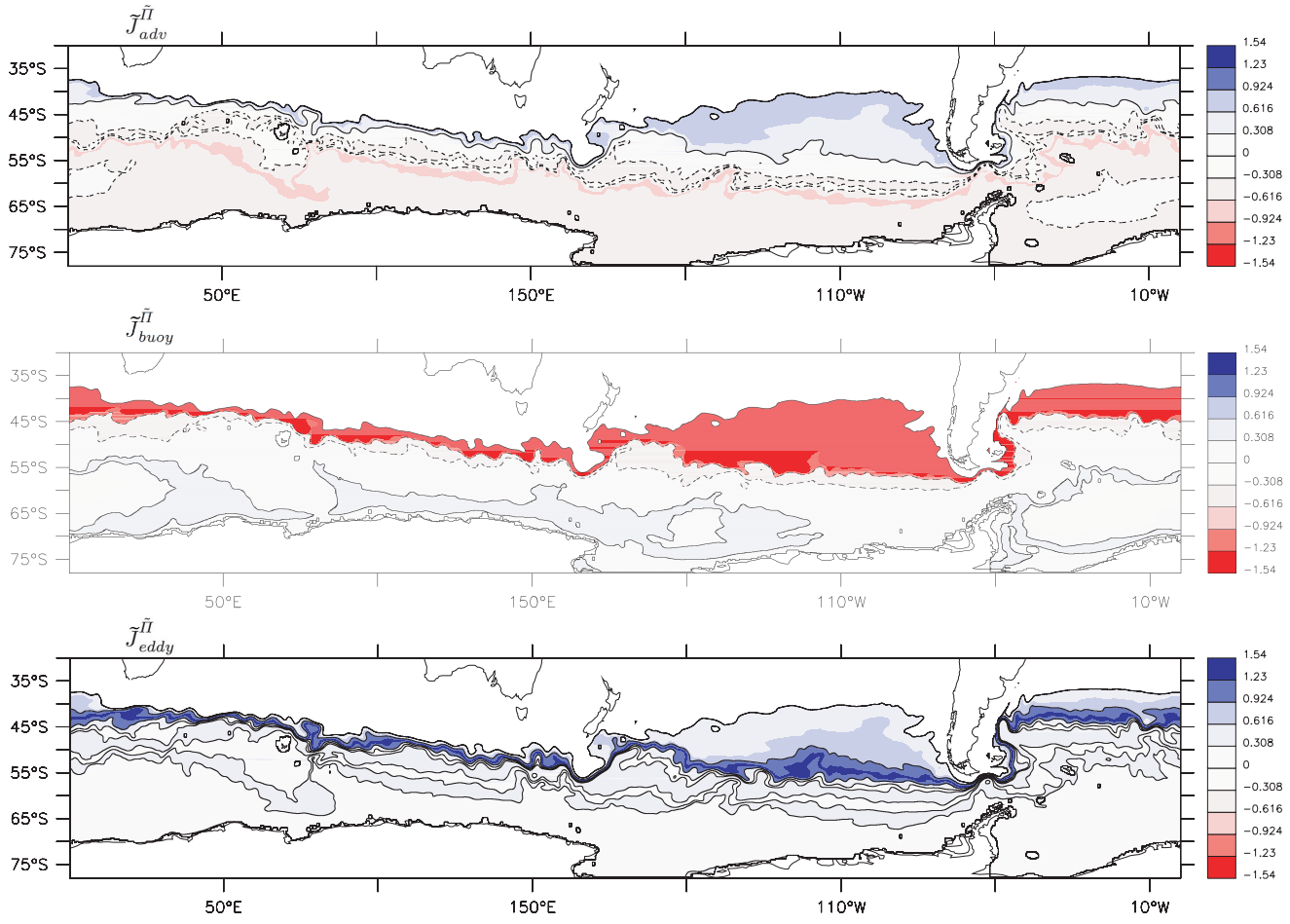

Fig. 7. Vertical fluxes of potential vorticity ($\times 10^{-13}\,\mathrm{kg\,m^{-3}\,s^{-2}}$) integrated over, and normalised by, the area between adjacent Bernoulli potential contours at 201 m depth in the Southern Ocean. Contours are parallel to Bernoulli contours and plotted every second shaded interval. Solid lines represent positive fluxes and dashed lines denote negative fluxes.

already been the subject of some discussion (Salmon, 1990; Marshall et al., 2002; Cessi and Fantini, 2004; Henning and Vallis, 2004; Radko and Marshall, 2004).

The potential vorticity flux integral constraint can address the nature of the diapycnal process in a gyre-averaged sense (that is along time-averaged closed Bernoulli contours). These diagnostics are presented at three depths, 52 m, 295 m and 1516 m, highlighting the three main regimes obtained for these fluxes. For reference, these depths are shown in Fig. 10, superimposed on a meridional section of σ. Again, note that the sign of the potential vorticity fluxes is reversed from the Southern Ocean due to the change in sign of the potential vorticity and is consistent with the limiting regimes discussion (Sect. 2.4).

5.1 52 m depth

First we consider a shallow depth lying within the winter mixed layer and hence subjected to surface buoyancy forcing (Fig. 11). There are two distinct regimes: (i) the inertial recirculation subgyre that is adjacent to the western boundary current, and (ii) the remainder of the gyre.

Within the inertial recirculation, the dominant balance is between the upward buoyancy-forced potential vorticity flux and the downward eddy-induced potential vorticity flux. This corresponds to the idealised limit sketched schematically in Fig. 3b in which the eddies are acting to restratify the mixed layer created through surface buoyancy loss. The advective potential vorticity flux is directed downward but is weak in magnitude compared with the other two terms. It is not surprising that the eddies play such a substantial role within the inertial recirculation since this is the centre of eddy activity in the gyre. Thus the overturning circulation within the inertial recirculation is dominated by the eddy-induced flux contribution, which is driven by surface buoyancy loss.

Over the remainder of the gyre, the dominant balance is between the advective potential vorticity flux and the

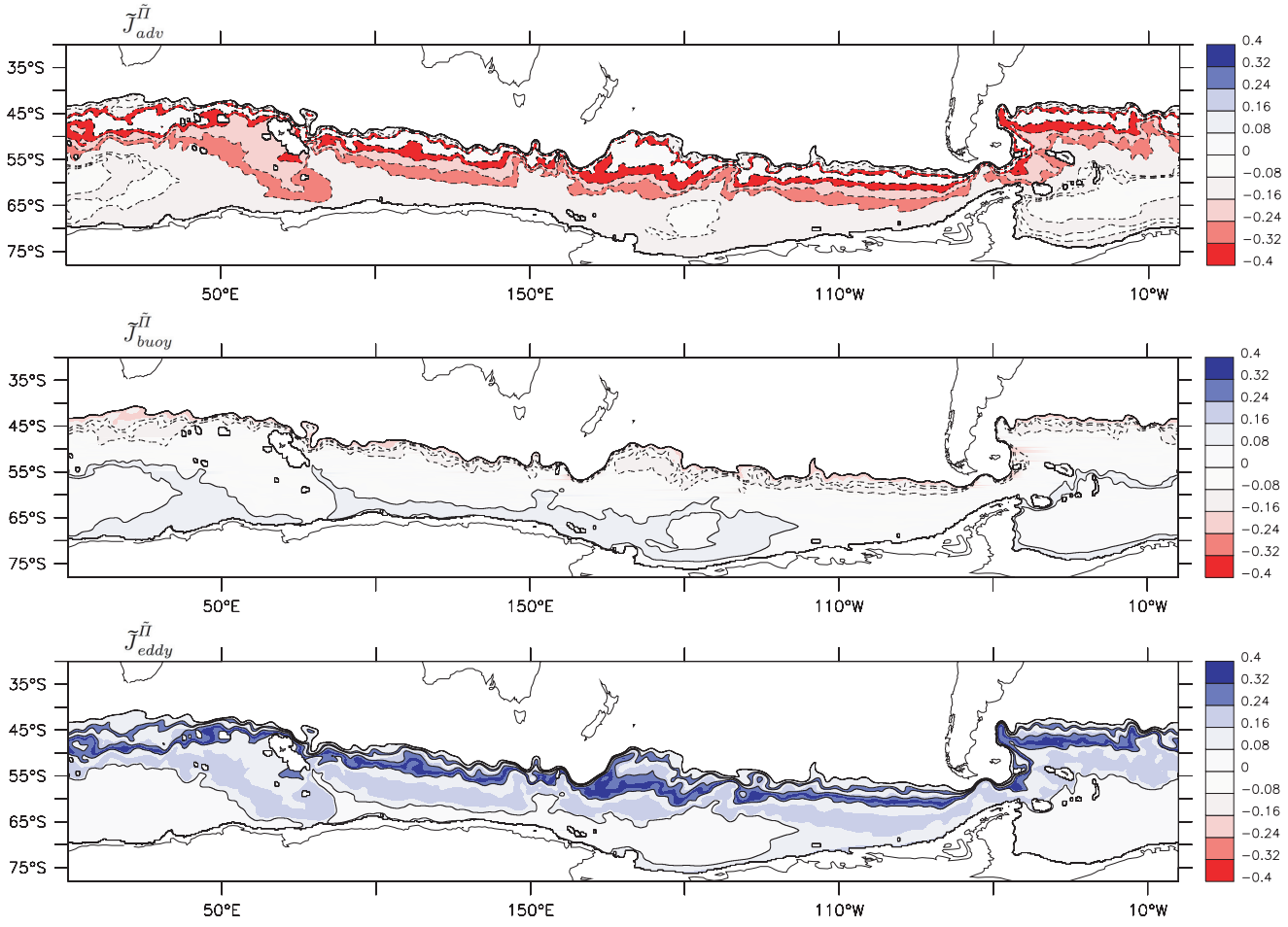

Fig. 8. Vertical fluxes of potential vorticity ($\times 10^{-13}\,\mathrm{kg\,m^{-3}\,s^{-2}}$) integrated over, and normalised by, the area between adjacent Bernoulli potential contours at 1150 m depth in the Southern Ocean. Contours are parallel to Bernoulli contours and plotted every second shaded interval. Solid lines represent positive fluxes and dashed lines denote negative fluxes.

buoyancy-forced potential vorticity flux. The advective flux is directed downward, due to the Eulerian-mean Ekman downwelling, whereas the buoyancy-forced potential vorticity flux is directed upward, consistent with net cooling. This cooling is required to compensate for the warm water being pumped downwards into the gyre. The eddy-induced potential vorticity flux is much weaker, and changes sign from downward in the centre of the gyre where it opposes the buoyancy forcing, to upward in the outer edges of the gyre where is starts to oppose Eulerian-mean downwelling.

5.2 295 m depth

We now consider an intermediate level lying within the main thermocline (Fig. 12). Here the dominant balance is between the advective potential vorticity flux and the buoyancy-forced potential vorticity flux. The downward advective potential vorticity flux represents the downward pumping of potential vorticity within the ventilated thermocline as described by Luyten et al. (1983). However, integrated over the gyre, this downward potential vorticity flux must be balanced by another process, which turns out to be neither eddy nor diffusive processes but to be buoyancy loss when the fluid parcels outcrop in the mixed layer within the northward flowing western boundary current.

The eddy-induced potential flux is generally (but not universally) directed upward, but is much weaker in magnitude than the advective potential vorticity flux. Thus compensation between the Eulerian-mean and eddy-induced overturning cells across the mean Bernoulli streamlines is only partial, and this compensation is far weaker than in the Southern Ocean. The one exception is within the inertial recirculation where the eddy-induced potential vorticity flux becomes comparable to the buoyancy-forced potential vorticity flux.

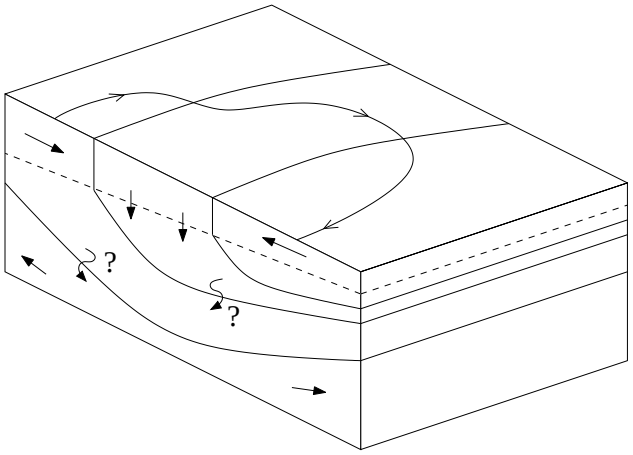

Fig. 9. Schematic of the residual overturning circulation across Bernoulli contours in a subtropical gyre. Unlike in the Southern Ocean Bernoulli contours do not approximately coincide with isopyncnic contours at constant depth. Hence water masses, with properties set in the mixed layer, must cross isopycnals in order to close the ageostrophic buoyancy budget.

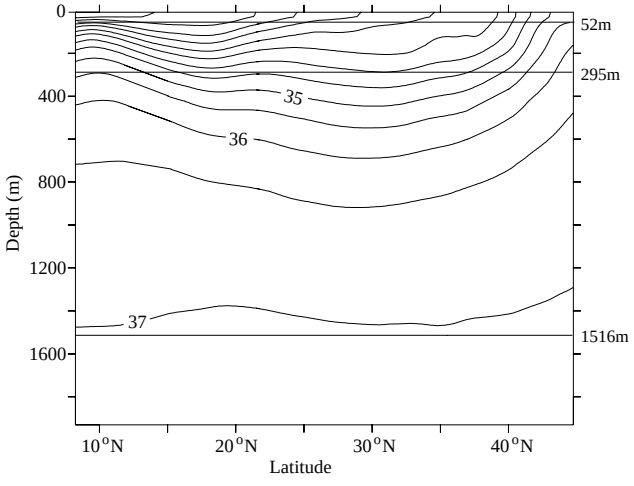

Fig. 10. A cross section of the mean σ through the North Pacific subtropical gyre at 160° E and the analysis levels at depths of 52 m, 295 m and 1516 m.

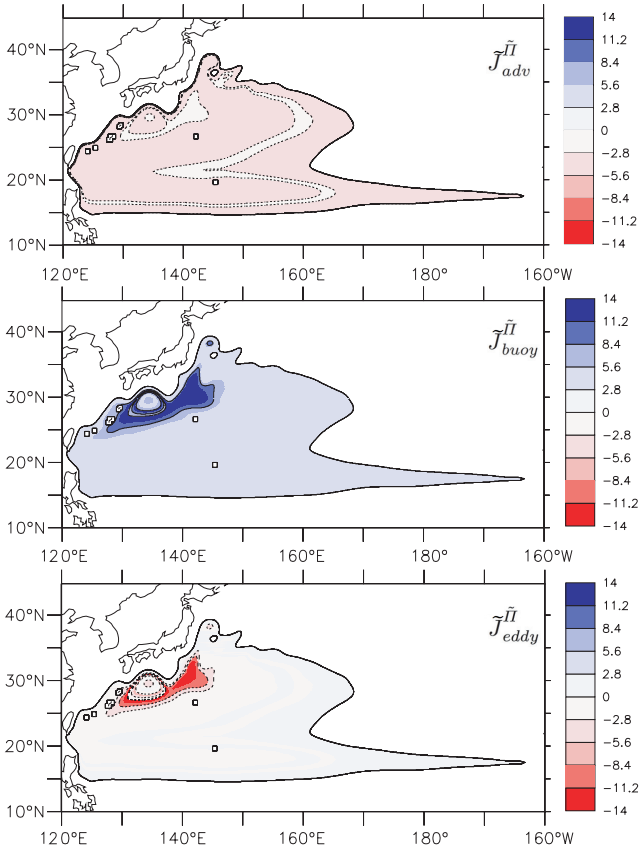

Fig. 11. Vertical fluxes of potential vorticity ($\times 10^{-13}$ kg m^{-3} s^{-2}) integrated over, and normalised by, the area between close closed Bernoulli potentials. Calculated at 52 m in the North Pacific subtropical gyre. Contours are parallel to Bernoulli contours and are plotted every second shaded interval. Solid lines represent positive fluxes and dashed lines denote negative fluxes.

5.3 1516 m depth

Finally we consider a deep level lying well beneath the main thermocline, in the upper part of the abyss (Fig. 13). The flow is cyclonic at this depth, and the potential vorticity fluxes are much weaker due both to the reduced vertical motion and the reduced stratification.

The dominant balance is again between the advective potential vorticity flux and the buoyancy-forced potential vorticity flux (though the signs of these fluxes reverse between the centre and outer edge of the gyre) with upwelling over the edge of the gyre and downwelling in the centre. The eddy-induced potential vorticity flux is small and of no consistent sign. The balance between the advective and buoyancy-forced potential vorticity fluxes actually holds locally (not shown).

The buoyancy-forced potential vorticity flux is dominated by the lateral diffusion of temperature, which acts to cool the centre of the gyre where the isopycnals are slightly depressed and to warm the outer edge of the gyre. The extent to which this process is an artifact of the numerical model, and hence not representative of a real ocean process, is unclear. One naturally wonders whether it is eddies and/or explicit diapycnal mixing that play the greater role in balancing the advective potential vorticity flux at such depths in the ocean.

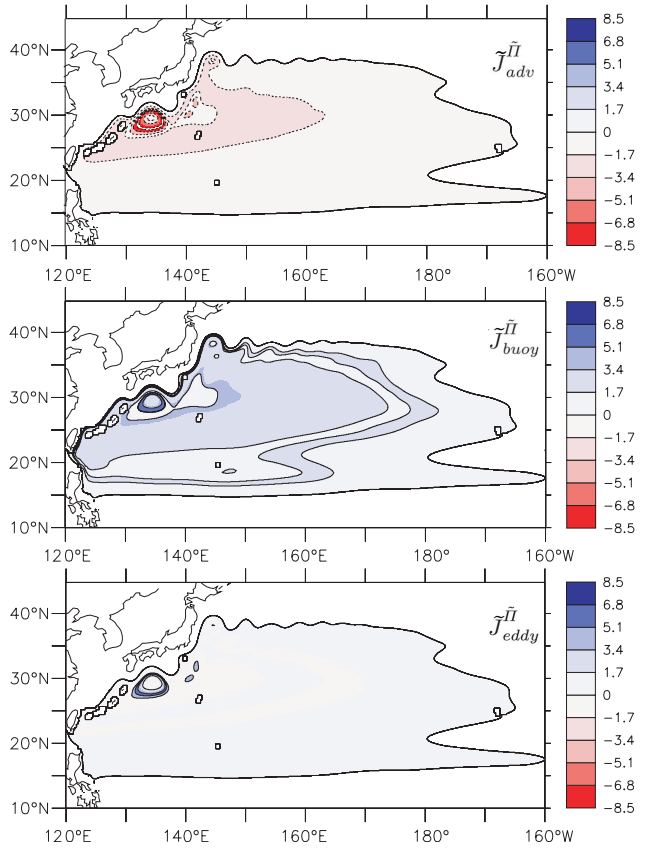

Fig. 12. Vertical fluxes of potential vorticity ($\times 10^{-13}\,\mathrm{kg\,m^{-3}\,s^{-2}}$) integrated over, and normalised by, the area between close closed Bernoulli potentials. Calculated at 295 m in the North Pacific subtropical gyre. Contours are parallel to Bernoulli contours and are plotted every second shaded interval. Solid lines represent positive fluxes and dashed lines denote negative fluxes.

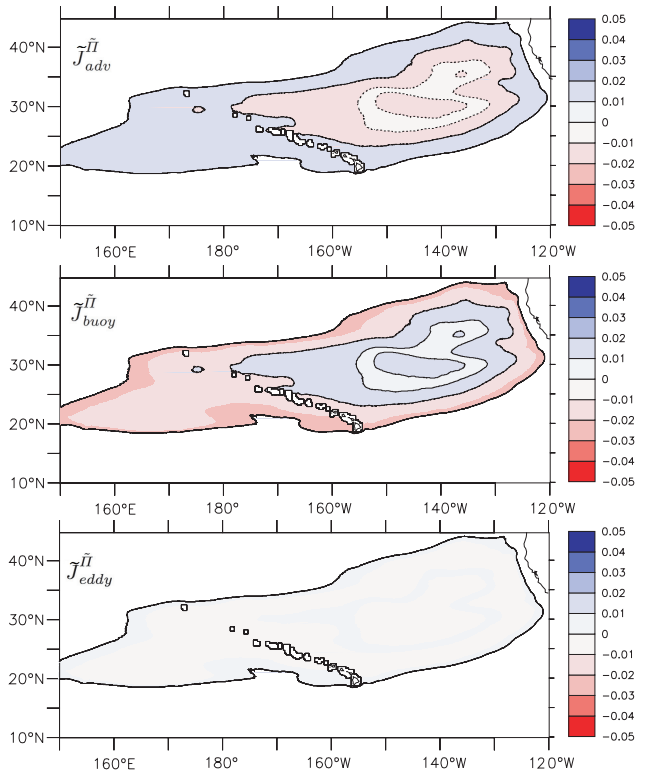

Fig. 13. Vertical fluxes of potential vorticity ($\times 10^{-13}\,\mathrm{kg\,m^{-3}\,s^{-2}}$) integrated over, and normalised by, the area between close closed Bernoulli potentials. Calculated at 1516 m in the North Pacific subtropical gyre. Contours are parallel to Bernoulli contours and are plotted every second shaded interval. Solid lines represent positive fluxes and dashed lines denote negative fluxes.

6 Discussion

We have developed a framework, based on an integral constraint on the vertical potential vorticity fluxes for a hydrostatic Boussinesq fluid, by which the circulation of a circumpolar current or an ocean gyre can be rigorously decomposed into a recirculating flow along closed Bernoulli potential contours and an overturning circulation across these contours.

We have presented diagnostics of the terms in the integral potential flux budget for both the ACC and North Pacific subtropical gyre in an eddy-permitting ocean circulation model, OCCAM.

Despite the apparent success in unifying Southern Ocean and subtropical dynamics here it should also be pointed out that there are significant differences in the dynamics and thermodynamics of the two regimes. For example, at the latitudes of the Drake Passage and above the bottom topography meridional geostrophic flow cannot be supported. Hence eddies are required meridionally resdistribute heat. Additionally, in classical Sverdrupian dynamics the mean flow is assumed to be small compared to the Rossby wave speed. The effect is that a succession of Rossby waves, of increasing vertical mode number, is able to confine the flow to the surface layers effectively decoupling the surface flow from the bottom topography. In the Southern Ocean, however, the mean flow is comparable to the fastest baroclinic Rossby wave speed and thus the Rossby waves are strongly influenced by the flow and the surface intensification of the circumpolar flow is prevented. This picture is consistent with surface observations in the ACC of eastward propagating anomalies of temperature and height (Hughes et al., 1998). Thus, in the Southern Ocean dynamics the role of topography cannot be neglected. In particular barotropic vorticity equation must be modified to include bottom pressure torque. Observational evidence (Gille, 1997; Stevens and Ivchenko, 1997; Rintoul et al., 2001) implies that windstress curl, when integrated over an area separated by more than 3-5 degrees of latitude, is balanced almost entirely by the bottom pressure torque. This contrasts with the classical Stommel gyre where a southward flow driven by a wind stress curl is returned in

a western boundary current that uses frictional a process to balance the vorticity budget. In the Southern Ocean a southward flow driven by a wind stress curl is anticipated to return north at locations determined by bottom pressure torque that satisfies the vorticity budget. For a more detailed discussion on the ACC and role of bottom topography see Rintoul et al. (2001) and Olbers (1998).

However, our diagnostics show both similarities and differences between the overturning cell in the Southern Ocean and the subtropical overturning cell in the North Pacific as represented in the OCCAM model. Both show a large compensation between the buoyancy-forced and eddy-induced potential vorticity fluxes within the surface mixed layer, and both show a distinct tendency for the eddy-induced potential vorticity flux to compensate to some extent the advective potential vorticity flux. However, this compensation is far greater in the Southern Ocean than in the subtropical gyre, except possibly within the inertial recirculation region where the eddies are stronger. This is undoubtedly due to the larger regions of intense eddy activity encountered by the Bernoulli contours in the Southern Ocean, whereas in the subtropical gyre the eddies are largely confined to the boundary current separation region. Additionally, in the subtropical gyre thermocline, we find that in a gyre-averaged sense the diapycnal mass flux is dominated by convective buoyancy forcing within the western boundary current region, rather than by diffusive or eddy processes. Whether all these findings carry over to ocean models with a better-resolved eddy field (and ultimately to the ocean) remains to be determined, but will be an interesting area for future study.

The diagnostic framework developed here can be applied to any flow in which there is a closed contour of Bernoulli potential, and so may find useful applications in other scenarios such as subpolar gyres or convective chimneys.

Acknowledgements. We are grateful to A. Coward and M.-M. Lee for supplying and helping us with the OCCAM data and to C. Hughes, A. Naveira Garabato and D. Webb for their constructive comments on the manuscript. Financial support was provided by the Natural Environment Research Council and by the Leverhulme Trust.

Edited by: S. M. Griffies

References

Cessi, P. and Fantini, M.: The eddy-driven thermocline, J. Phys. Oceanogr., 34, 2642–2658, 2004.

Danabasoglu, G., McWilliams, J. C., and Gent, P. R.: The Role of Mesoscale Tracer Transports in the Global Ocean Circulation, Science, 264, 1123–1126, 1994.

Döös, K. and Webb, D. J.: The Deacon Cell and the Other Meridional Cells of the Southern Ocean, J. Phys. Oceanogr., 24, 429–442, 1994.

Drijfhout, S. S.: What Sets the Surface Eddy Mass Flux in the Southern Ocean?, J. Phys. Oceanogr., 35, 2152–2166, 2005.

Eliassen, A. and Palm, E.: On the transfer of energy in stationary mountain waves, Geofys. Publ., 22, 1–23, 1961.

Gallego, B., Cessi, P., and McWilliams, J. C.: The Antarctic Circumpolar Current in Equilibrium, J. Phys. Oceanogr., 34, 1571–1587, 2004.

Gent, P. R., Willebrand, J., McDougall, T. J., and McWilliams, J. C.: Parameterizing eddy-induced tracer transports in ocean circulation models, J. Phys. Oceanogr., 25, 463–474, 1995.

Gille, S. T.: The Southern Ocean Momentum Balance: Evidence for Topographic Effects from Numerical Model Output and Altimeter Data, J. Phys. Oceanogr., 27, 2219–2232, 1997.

Haynes, P. H. and McIntyre, M. E.: On the Evolution of Vorticity and Potential Vorticity in the Presence of Diabatic Heating and Frictional or Other Forces, J. Atmos. Sci., 44, 828–841, 1987.

Haynes, P. H. and McIntyre, M. E.: On the Conservation and Impermeability Theorems for Potential Vorticity, J. Atmos. Sci., 47, 2021–2031, 1990.

Henning, C. C. and Vallis, G. K.: The Effects of Mesoscale Eddies on the Main Subtropical Thermocline, J. Phys. Oceanogr., 34, 2428–2443, 2004.

Hughes, C. W., Jones, M. S., and Carnochan, S. A.: Use of transient features to identify eastward currents in the Southern Ocean, J. Geophys. Res., 103, 2929–2944, 1998.

Johnson, G. C. and Bryden, H. L.: On the size of the Antarctic Circumpolar Current, Deep-Sea Res., 36, 39–53, 1989.

Karsten, R., Jones, H., and Marshall, J.: The role of eddy transfer in setting the stratification and transport of a Circumpolar Current, J. Phys. Oceanogr., 32, 39–54, 2002.

Karsten, R. H. and Marshall, J.: Constructing the residual circulation of the ACC from observations, J. Phys. Oceanogr., 32, 3315–3327, 2002.

Luyten, J. R., Pedlosky, J., and Stommel, H.: The Ventilated Thermocline, J. Phys. Oceanogr., 13, 292–309, 1983.

Marshall, D. P.: Subduction of water masses in an eddying ocean, J. Mar. Res., 55, 201–222, 1997.

Marshall, D. P.: Vertical Fluxes of Potential Vorticity and the Structure of the Thermocline, J. Phys. Oceanogr., 30, 3102–3112, 2000.

Marshall, D. P., Williams, R. G., and Lee, M.-M.: The relation between eddy-induced transport and isopycnic gradients of potential vorticity, J. Phys. Oceanogr., 29, 1571–1578, 1999.

McDougall, T. J.: Neutral Surfaces, J. Phys. Oceanogr., 17, 1950–1964, 1987.

Marshall, J., Jones, H., Karsten, R., and Wardle, R.: Can eddies set ocean stratification?, J. Phys. Oceanogr., 32, 26–38, 2002.

Obukhov, A. M.: On the dynamics of a stratified liquid, Dokl. Akad. Nauk SSSR, 145, 1239–1242, (English: 1963, Sov. Phys. Dolk., 7(8), 682–684), 1962.

Olbers, D.: Comments on "On the Obscurantist Physics of "Form Drag" in Theorizing about the Circumpolar Current", J. Phys. Oceanogr., 28, 1647–1654, 1998.

Olbers, D., Borowski, D., Völker, C., and Wölff, J.-O.: The dynamical balance, transport and circulation of the Antarctic Circumpolar Current, Antarctic Science, 16, 439–470, 2004.

Plumb, R. A.: A Nonacceleration Theorem for Transient Quasi-geostrophic Eddies on a Three-Dimensional Time-Mean Flow, J. Atmos. Sci., 47, 1825–1836, 1990.

Polton, J. A. and Marshall, D. P.: Understanding the structure of the subtropical thermocline, J. Phys. Oceanogr., 33, 1240–1249,

2003.

Radko, T. and Marshall, J.: The Leaky Thermocline, J. Phys. Oceanogr., 34, 1648–1662, 2004.

Rintoul, S. R., Hughes, C. W., and Olbers, D.: Ocean Circulation and Climate: Observing and modelling the global ocean, chap. 4.6, Acedemic Press, 2001.

Roberts, M. J. and Marshall, D. P.: On the Validity of downgradient eddy closures in ocean models, J. Geophys. Res., 105, 28 613–28 627, 2000.

Salmon, R.: The Thermocline as an "internal boundary layer", J. Mar. Res., 48, 437–469, 1990.

Schmitz, W. J.: On the World Ocean Circulation: Volume II. The Pacific and Indian Oceans / A global update, Woods Hole Oceanog. Inst. Tech. Rept., WHOI-96-08, pp245, 1996.

Speer, K., Rintoul, S. R., and Sloyan, B.: The Diabatic Deacon Cell, J. Phys. Oceanogr., 30, 3212–3222, 2000.

Stevens, D. P. and Ivchenko, V. O.: The Zonal Momentum Balance in an Eddy Resolving General Circulation Model of the Southern Ocean, Quart. J. Roy. Meteor. Soc., 123, 929–951, 1997.

Treguier, A. M., Held, I. M., and Larichev, V. D.: Parameterization of Quasigeostrophic Eddies in Primitive Equation Ocean Models, J. Phys. Oceanogr., 27, 567–580, 1997.

Truesdell, C.: Proof that Ertel's vorticity theorem holds in average for any medium suffering no tangential acceleration on the boundary, Geofis. Pura Appl., 19, 167–169, 1951.

Webb, D. J., de Cuevas, B. A., and Coward, A. C.: The first main run of the OCCAM global ocean model, Tech. rep., SOC Internal document No. 34, James Rennell Division, Southampton Oceanography Centre, S014 3ZH, UK, 43 pp, 1998.

White, A. A. and Bromley, R. A.: Dynamically consistent, quasi-hydrostatoc equations for global models with a complete representation of the Coriolis force, Q. J. R. Meteorol. Soc., 121, 399–418, 1995.